Annals of Biomedical Engineering, Vol. 41, No. 2, February 2013 (© 2012) pp. 263–278
DOI: 10.1007/s10439-012-0640-2

BMES BIOMEDICAL ENGINEERING SOCIETY™ www.bmes.org

Hemodynamically Motivated Choice of Patch Angioplasty for the Performance of Carotid Endarterectomy

ALEXEY V. KAMENSKIY,[1] JASON N. MACTAGGART,[1] IRAKLIS I. PIPINOS,[1] PRATEEK K. GUPTA,[2] and YURIS A. DZENIS[3]

[1]Department of Surgery, University of Nebraska-Medical Center, 985182 Nebraska-Medical Center, Omaha, NE 68198-5182, USA; [2]Creighton University Medical Center, Omaha, NE, USA; and [3]Department of Mechanical & Materials Engineering, University of Nebraska-Lincoln, Lincoln, NE 68588, USA

(*Received 27 April 2012; accepted 10 August 2012; published online 25 August 2012*)

Associate Editor Jane Grande-Allen oversaw the review of this article.

Abstract—Patch angioplasty is the most common technique used for the performance of carotid endarterectomy. A large number of materials are available, but little is known to aid the surgeon in choosing a patch while caring for a patient with carotid disease. The objective of this study was to investigate biomechanics of the carotid artery (CA) repaired with patch angioplasty, study the influence of patch width and location of closure on hemodynamics, and to select the optimal patch material from those commonly used. For this purpose, a mathematical model was built that accounts for fluid–structure interaction, three-dimensional arterial geometry, non-linear anisotropic mechanical properties, non-Newtonian flow and *in vivo* boundary conditions. This model was used to study disease-related mechanical factors in the arterial wall and blood flow for different types of patch angioplasty. Analysis indicated that patch closures performed with autologous vein and bovine pericardium were hemodynamically superior to carotid endarterectomy with synthetic patch angioplasty (polytetrafluoroethylene, Dacron) in terms of restenosis potential. Width of the patch and location of arteriotomy were found to be of paramount importance, with narrow patches being superior to wide patches, and anterior arteriotomy being superior to the lateral arteriotomy. These data can aid vascular surgeons in their selection of patch angioplasty technique and material for the care of patients undergoing open CA repair.

Keywords—Carotid artery, Endarterectomy, Patch angioplasty, Finite element analysis, Hemodynamics, Atherosclerosis, Restenosis.

Address correspondence to Alexey V. Kamenskiy, Department of Surgery, University of Nebraska-Medical Center, 985182 Nebraska-Medical Center, Omaha, NE 68198-5182, USA and Yuris A. Dzenis, Department of Mechanical & Materials Engineering, University of Nebraska-Lincoln, Lincoln, NE 68588, USA. Electronic mail: Alexey.Kamenskiy@unmc.edu, ydzenis@unl.edu

INTRODUCTION

Atherosclerosis of the carotid artery (CA) bifurcation is a leading cause of stroke. Endarterectomy (CEA) has been shown to significantly reduce the risk of stroke in patients with severe carotid bifurcation stenosis.[3,39,43] The standard approach for the performance of CEA involves a longitudinal arteriotomy from the common (CCA) to the internal carotid artery (ICA) followed by removal of the atherosclerotic plaque. There is significant clinical evidence that closing the longitudinal arteriotomy after CEA using a patch is superior to common primary closure in reducing the risk of restenosis and improving both short and long term clinical outcomes.[1,5,9,17,40,44]

Autologous vein (either greater saphenous or external jugular) was the first material to be used as carotid patch. Vein provides an endothelialized surface to the reconstructed arterial segment, is relatively readily available, easy to handle, and has high resistance to infection. Its main disadvantage is the need for an additional incision to obtain it, and occasional deterioration with aneurismal dilatation and rupture. In addition to vein, a number of xenogeneic and synthetic patches are now available. Xenogeneic patches are made of bovine pericardium (BP), while synthetic patches are made mostly of polytetrafluoroethylene (PTFE) or Dacron. The advantages of prosthetic patches include immediate availability, avoidance of additional incision, and preservation of vein for future use in other cardiovascular operations. The main shortcoming of the prosthetic patches is higher thrombogenicity and increased risk for infection.

Despite the broad range of available materials, there is currently minimal data to aid the surgeon in

choosing a patch while caring for a patient with carotid disease. In addition, limited information is available on whether location of arteriotomy and the width of the patch have significant impact on the hemodynamics of the repaired artery. The study of the biomechanical behavior of the patched CA may help answering these questions and defining the patch of choice among those currently available. Such study is best performed with the help of mathematical modeling.

In recent years mathematical modeling of arteries has matured immensely with the emergence of better imaging, mesh generation, computation, and visualization technologies. State-of-the-art models incorporate fully coupled fluid–structure interaction, and account for substantial arterial wall non-linearity. Such simulations are done in an effort to investigate certain hemodynamic factors that influence the onset and progression of cardiovascular disease. These factors include stresses and strains in the arterial wall and the blood flow,[11,12,15,35,51,54,56] which are thought to be related to arterial disease through hemodynamic (low shear)[11,20] and injury[15,46] mechanisms.

The hemodynamic mechanism of atherogenesis was initially postulated by Fry[20] and Caro *et al.*[11] They noticed that the natural widening of the carotid bulb and the branching into the ICA and external carotid artery (ECA) perturb the normal laminar flow present in the more proximal CCA. Flow alterations occur in both the longitudinal and transverse directions. In the longitudinal direction, flow in the bulb is partially reversed and the boundary layer is separated. In the transverse direction, flow undergoes considerable rotation (a condition known as secondary flow). Both boundary layer separation and secondary flow result in vortices, low and oscillatory wall shear stress (WSS), and higher time of platelet residence. This is thought to increase the permeability of the endothelium by ceasing production of Nitric Oxide,[53] and also the proteins that form the junctions between the endothelial cells.[16] In turn, this may lead to adhesion of monocytes to the endothelium, and development of the atherosclerotic plaque.[35]

The injury mechanism of atherogenesis was first described by Ross[46] and Clowes *et al.*[15] They hypothesized that damage of the arterial wall can lead to cell migratory and proliferative responses. Following platelet deposition this may result in slow accumulation of lipoproteins and development of arterial disease.[38] Mechanical injury to the arterial wall can be induced by high cyclic strains (CS) and excessive stresses.[15,51,54,56]

In the context of these two theories special attention has been given to models of healthy[37,56] and severely diseased arteries,[18,34,52] yet surprisingly little consideration was given to studies of the endarterectomized and patched carotids.[31] The goal of the present work was to investigate the biomechanics of such arteries, study the influence of patch width and location of arteriotomy on hemodynamics, and to select the optimal patch material that could minimize restenosis.

METHODS

Sixteen consecutive male patients with severe CA atherosclerotic disease (>80% diameter reduction as determined per North American Symptomatic Carotid Endarterectomy Trial (NASCET) criteria[19] using Computerized Tomography Angiography), who subsequently underwent CEA, were selected for this study. Informed consent was obtained from each patient in accordance with regulations established by the institutional review board of our institute.

Arterial Geometry

Computer reconstruction of CA geometry was based on preoperative Computerized Tomographic Angiography data obtained with 64-channel scanner Brilliance 64 (Philips Medical Systems, Cleveland, OH). Details of reconstruction and analysis can be found in Kamenskiy *et al.*[30] Briefly, two-dimensional cross-sectional data of 100 mm CA segment (5 cm distal into the ICA and 5 cm proximal into the CCA off the carotid apex, i.e., axial location where CCA divides into the ICA and ECA (see Fig. 1) were acquired with axial steps of 1 mm and spatial resolution of 512 × 512 pixels (pixel size 0.488 mm). The images were rescaled to 1200 × 1200 pixel matrix size (pixel size 0.208 mm) using sub-pixel interpolation which helped in the segmentation of the outer (periadventitial) and inner (luminal) boarders of the CCA, ICA and ECA.[49] Segmentation was performed in a semi-automatic manner under the supervision of a vascular surgeon who reviewed each result produced by the algorithm and corrected the segments of the automatically detected boundary that were partially obscured by periadventitial fat, atherosclerotic plaque or were ill-defined due to poor contrast. After segmentation, best fit ellipses were inscribed in each of the arterial contours. This procedure was performed for each of the 16 patients in the group. Subsequently, the mean contours were calculated by averaging the individual patient geometrical data sets.[30] This averaging resulted in a stack of mean arterial cross-sections that were connected together to form the three-dimensional solid body of the mean CA in Computer Aided Design software Solid Works (Dassault Systemes SolidWorks Corporation, Concord, Massachusetts) using the loft function. We note that segmentation in the apex area

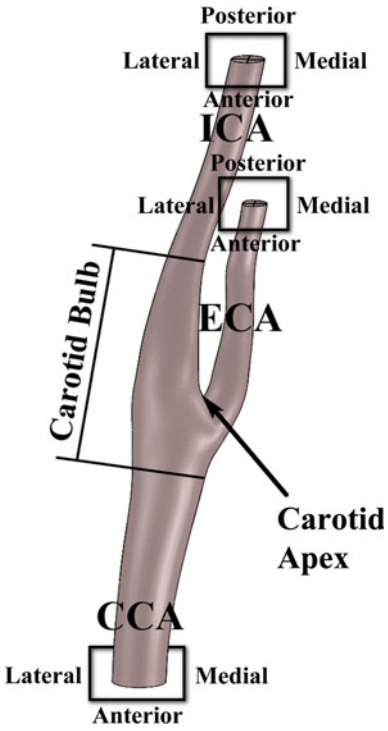

FIGURE 1. Scheme of the carotid artery bifurcation showing carotid bulb, apex and conventions on orientations (anterior–posterior, lateral-medial) for common (CCA), internal (ICA) and external (ECA) carotid arteries.

required special attention because branching perturbed the centroids of the vessels causing perturbations of the centroid path. To resolve this issue, we built the CCA-ICA and CCA-ECA segments separately and then merged them together in Solid Works. Distal branches of the ECA were excluded from analysis because of their small size.

The arterial geometry was further modified in Solid Works to simulate CEA with patch angioplasty. Three different patch widths were considered: narrow (4 mm), standard (8 mm) and wide (16 mm). The thickness of the wall in the endarterectomized area was made half of that of the normal wall to account for the removal of intima and part of media during CEA.[31] In addition, 0.5 mm of material (arterial wall and patch) was removed from both sides of the arteriotomy to account for the stitch.

Mathematical Model

Coupled fluid–structure boundary value problem was set up through separate mathematical descriptions in each of the fluid and solid domains. Unstructured meshes were used due to the complex geometries involved. The Octree method[6] was used to mesh the domains, and to facilitate reasonable approximations in the boundary later. Due to stability considerations, 11-node tetrahedral quadratic elements with mixed u/p formulation were used for the nearly incompressible arterial wall,[6,56] while 4-node linear elements were used for the blood flow. Mesh convergence for both fluid and solid domains was studied, and the appropriate mesh size was selected such that further refinement resulted in less than 5% difference in WSS and effective stress (ES) (see their definitions below). This resulted in approximately 150 000 fluid, and 115 000 solid elements.

Arbitrary Lagrangian–Eulerian formulation for the conservation of mass and momentum equations for the fluid was used to account for the movement of the fluid mesh at the boundary with the solid domain. This was achieved by replacing the material velocity $\mathbf{u}$ which appears in the convective term of Eulerian formulations with a convective velocity $(\mathbf{u} - \mathbf{u_g})$:

$$\nabla \cdot \mathbf{u} = 0 \tag{1}$$

$$\rho_f \left(\frac{\partial \mathbf{u}}{\partial t} + \left((\mathbf{u} - \mathbf{u_g}) \cdot \nabla \right) \mathbf{u} \right) = -\nabla p_f + \nabla \cdot \boldsymbol{\tau} \tag{2}$$

where ρ_f is fluid density, p_f is pressure, $\mathbf{u}$ is the fluid velocity vector and $\mathbf{u_g}$ is the moving coordinate velocity (mesh velocity), so $(\mathbf{u} - \mathbf{u_g})$ is the relative velocity of the fluid with respect to the moving coordinate velocity. Further, $\boldsymbol{\tau}$ is the fluid stress tensor, related to rate-of-deformation tensor $\mathbf{D}$ as

$$\boldsymbol{\tau} = 2\mu \mathbf{D} = \mu(\nabla \mathbf{u} + (\nabla \mathbf{u})^T) \tag{3}$$

where μ is blood viscosity. Blood was modeled as a non-Newtonian fluid with μ changing according to the Carreau constitutive law. This law was reported to accurately describe the shear thinning rheological behavior of blood in arteries[28]:

$$\mu = \mu_\infty + (\mu_0 - \mu_\infty)\left(1 + A\dot{\gamma}^2\right)^m \tag{4}$$

where μ_0 and μ_∞ are upper and lower bounds of viscosity, A and m are parameters and $\dot{\gamma} = \sqrt{2\mathbf{D} : \mathbf{D}}$ is the scalar shear rate. Experimental blood rheology was beyond the scope of this study, and commonly used values of constitutive parameters were taken from Cho and Kensey[14]: $\mu_0 = 0.056$ Pa s, $\mu_\infty = 0.00345$ Pa s, A = 10.976 s^2, $m = -0.3216$. We note that a different value of $\mu_0 = 0.16$ Pa s obtained by Chien[13] is also quite commonly used in the literature, which needs to be kept in mind when comparing the results obtained by different research groups. Density of blood was assumed constant: $\rho_f = 1050$ kg/m^3.

Momentum conservation equation in the Lagrangian description with large displacements and large strains was solved for the solid domain:

$$\nabla \cdot \boldsymbol{\sigma_s} = \rho_s \ddot{\boldsymbol{d}}_s \tag{5}$$

TABLE 1. Constitutive model parameters C_1, k_1, k_2, γ calculated for the mean carotid artery wall and vascular patches.

Material	C_1 (kPa)	k_1 (kPa)	k_2	γ (rad)
Carotid artery wall	41	3	14	0.90
External jugular vein	98	77	67	0.60
Greater saphenous vein	92	86	61	0.65
BP (by Synovis and NeoVasc)	119	337	115	0.68
Acuseal polytetrafluorethylene (by GORE)	2485	–	–	–
Dacron Hemacarotid (by GORE)	3429	–	–	–
Dacron Hemashield (by Boston Scientific)	3778	–	–	–

where ρ_s is density of the solid, $\boldsymbol{\sigma}_\mathbf{s}$ is the solid stress tensor, and $\ddot{\mathbf{d}}_\mathbf{s}$ is the local acceleration of the solid.

Arterial wall and vascular patches were assumed homogeneous, incompressible and hyperelastic with strain energy taken in the HGO (Holzapfel, Gasser, Ogden[23]) form:

$$W(\mathbf{C}, \hat{\mathbf{n}}_a, \hat{\mathbf{n}}_b) = W_{\text{iso}}(\mathbf{C}) + W_{\text{anis}}(\mathbf{C}, \hat{\mathbf{n}}_a, \hat{\mathbf{n}}_b) \quad (6)$$

where $W_{\text{iso}}(\mathbf{C}) = C_1(I_1 - 3)$ is the isotropic part of the strain energy function W and $W_{\text{anis}}(\mathbf{C}, \hat{\mathbf{n}}_a, \hat{\mathbf{n}}_b) = \frac{k_1}{2k_2} \sum_{i=4,6} \left\{ e^{k_2(I_i-1)^2} - 1 \right\}$ describes the anisotropic part of W. $I_i \geq 1$ are the invariants of the right Cauchy-Green deformation tensor $\mathbf{C} = \mathbf{F}^T\mathbf{F}$ (note that $I_{4,6} \geq 1$ are required for physically reasonable response[23]); C_1, k_1, k_2 are positive[23] constitutive model parameters, and $\hat{\mathbf{n}}_a, \hat{\mathbf{n}}_b$ are unit vectors (with angle 2γ between them) in reference configuration that define anisotropy. Orientation of vectors $\hat{\mathbf{n}}_a, \hat{\mathbf{n}}_b$ for each element of the model was set up by dividing the entire three-dimensional geometry into simple sub-volumes, for each of which the orientation could be easily defined using the bounding outer surface.

Cauchy stress tensor $\boldsymbol{\sigma}_\mathbf{s}$ was then calculated from (6) as

$$\begin{aligned}\boldsymbol{\sigma}_\mathbf{s} &= -p\mathbf{I} + \mathbf{F}\frac{\partial W}{\partial \mathbf{F}} = -p\mathbf{I} + 2\frac{\partial W}{\partial I_1}\mathbf{B} + 2\frac{\partial W}{\partial I_2}\left(I_1\mathbf{B} - \mathbf{B}^2\right) \\ &+ 2\frac{\partial W}{\partial I_4}\mathbf{F}\hat{\mathbf{n}}_a \otimes \mathbf{F}\hat{\mathbf{n}}_a = -p\mathbf{I} + C_1\mathbf{B} + 4k_1(I_4 - 1) \\ &\times \exp\left[k_2(I_4 - 1)^2\right](\mathbf{F}\hat{\mathbf{n}}_a \otimes \mathbf{F}\hat{\mathbf{n}}_a) \quad (7)\end{aligned}$$

where $\mathbf{F}$ is the deformation gradient tensor, $\mathbf{B} = \mathbf{F}\mathbf{F}^T$ is the left Cauchy–Green tensor, and p is Lagrange multiplier associated with the incompressibility constraint $\det\mathbf{F} = 1$.

Values of constitutive model parameters C_1, k_1, k_2, γ for the arterial wall and patches were determined by fitting (7) to the experimental data of Kamenskiy *et al.*[32] using Levenberg–Marquardt algorithm. Parameters C_1, k_1, k_2, γ were required to be positive in order to portray physically reasonable response.[23] This guaranteed the convexity of the strain energy potential (6) for any given set of parameters.[23] Values of these parameters for the mean carotid artery wall and patches are summarized in Table 1. Neo-Hookean material (isotropic part of (6)) was used for synthetic patches due to their linear isotropic behavior in the physiological load range.[32]

Galerkin procedure was used to discretize both the fluid and solid governing equations and establish their weak forms. Discrete equations were then solved using Newton's method and direct sparse solver based on the Gauss elimination technique.[6] To achieve a periodic solution, computation was run over two cardiac cycles, saving only the second one. Initially, three cardiac cycles were calculated, but comparison of the parameters of interest between the second and third cycles revealed that two cardiac cycles were sufficient to obtain periodicity. Each cardiac cycle consisted of 500 time steps of 2×10^{-3} s, and automatic-time-stepping procedure[6] was used to subdivide the load step increment when necessary.

Boundary Conditions

Boundary conditions included the actual *in vivo* measured pulsatile velocity profiles (temporal and spatial variations of velocity) in the distal ICA and ECA, and concurrently measured pressure waveform (temporal variation of pressure) in the proximal CCA. Both the velocity and the pressure were obtained intraoperatively after completion of the CEA for the same group of 16 patients, and then reduced to correspond with the mean geometry. Duplex ultrasound (Pro Focus 2202, Probe 8809; B-K Medical, Herlev, Denmark) was used for measurement of the carotid artery blood flow. Details of these measurements and reduction are provided in Kamenskiy *et al.*[29] A snapshot of mean velocity profiles at peak systole and late diastole are illustrated in Fig. 2.

Mean profiles were then applied to the ICA and ECA out-flow sections as kinematic boundary conditions using custom Matlab code. This code interpolated the kinematic values of velocity for each node of the ICA and ECA out-flow sections and generated temporal velocity functions for each of these nodes. Pressure waveform was applied to the in-flow section of the CCA.

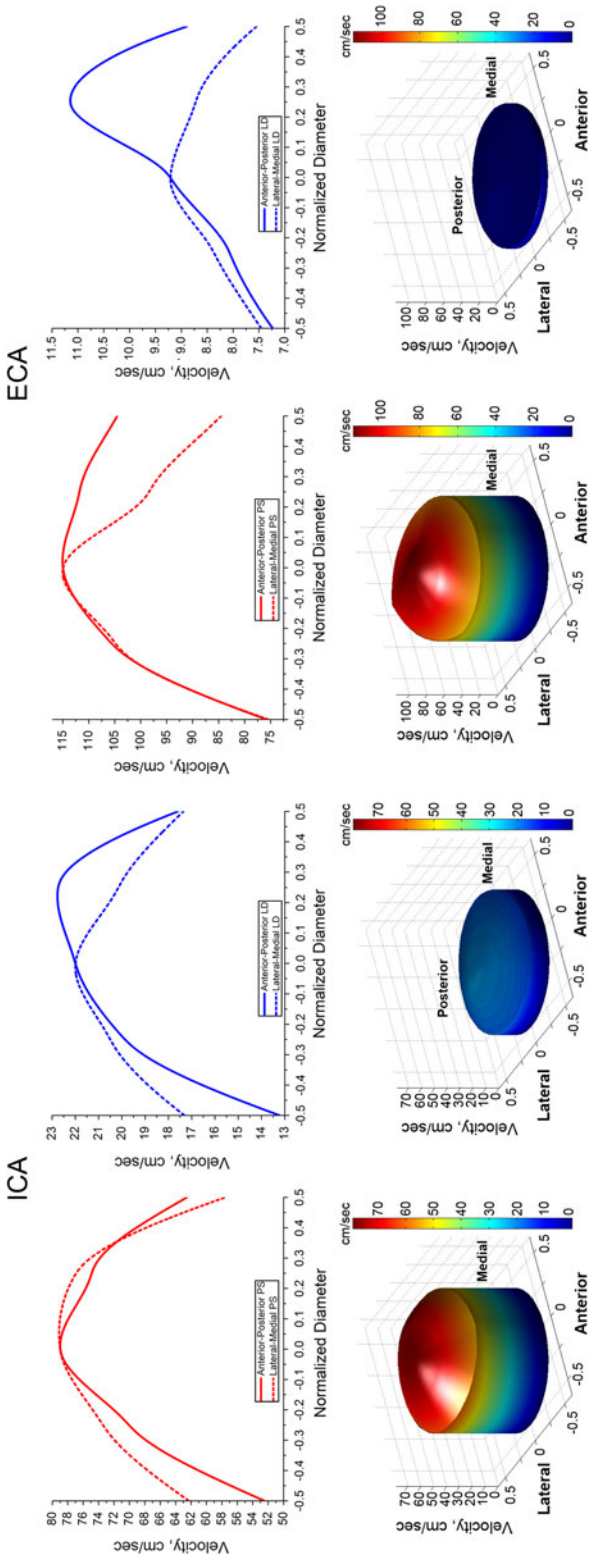

FIGURE 2. Variation of axial velocity along the anterior–posterior and lateral-medial directions of the lumen (top) and 3D axial velocity profiles assigned to the outlets of the ICA and ECA (bottom). Figures are plotted for peak systole (time of maximum flow, red graph) and late diastole (end of cardiac cycle, blue graph).

Motion of the fluid boundary along with the solid wall, conservation of mass, momentum and mechanical energy on the interface were fulfilled by imposing the kinematic and dynamic conditions on the interface between the blood flow and the arterial wall. Those included compatibility of displacements of the fluid and solid domains ($\mathbf{d_s} = \mathbf{d_f}$), equilibrium of tractions on the interface ($\hat{\mathbf{n}} \cdot \boldsymbol{\sigma}_\mathbf{s} = \hat{\mathbf{n}} \cdot \boldsymbol{\tau}$, where $\hat{\mathbf{n}}$ is a unit boundary normal), and no-slip conditions for the blood flow ($\mathbf{u} = \dot{\mathbf{d}}_\mathbf{s}$).

Coupling was achieved by passing fluid stress at the boundary to the structural solver (ADINA Structures, Watertown, Massachusetts) as an applied load. After finding the structural solution, the structural solver returned the resulting boundary displacements to the fluid solver (ADINA CFD, Watertown, Massachusetts), providing the latter with updated flow geometry. Flow geometry was updated through transfinite interpolation and nodal constraints. The iterative process continued at each time step until solutions at the boundary were sufficiently compatible.[25]

Introduction of Surgical Suture and Patch

The surgical suture was introduced into the model as rigid links connecting neighboring Finite Element nodes on both sides of the arteriotomy. Rigid links are constraint equations established between the two nodes—master and slave. As nodes get displaced due to deformation, the slave node is constrained to translate in such a way that its distance to the master node remains constant. Master nodes were selected to belong to the arterial wall, while slave nodes belonged to the patch. The nodes were selected such that the gap between the suture bites was approximately 0.8 mm as recommended by patch manufacturers (see Fig. 3). The suture was simulated on the outer and inner surfaces of the artery mimicking the actual surgical procedure. In addition to rigid links, simple non-penetrating rigid contact was implemented between the patch and the arterial wall to ensure simultaneous movement of the two bodies. The described procedure allowed to significantly reduce the computational time required to suffice the refined meshes around the suture entry site in the arterial wall.

Analysis of Disease-Related Mechanical Factors

Carotid arteries repaired with various types of patch angioplasty were compared to each other in terms of arterial disease-related mechanical factors, namely WSS, Oscillatory Shear Index (OSI), endothelial platelet residence time (T_r), CS, and ES.[11,12,15,35,51,54,56]

WSS was evaluated as the temporal mean during the complete cardiac cycle to provide the average hemodynamic effect indicator. Calculation of WSS involved multiplication of the dynamic viscosity with the velocity gradient projected onto the luminal surface and calculated in the direction of local unit surface normal $\hat{\mathbf{n}}_\mathrm{s}$:

$$\boldsymbol{\tau}_\mathrm{s} = \mu \frac{\partial \mathbf{u}}{\partial \hat{\mathbf{n}}_\mathrm{s}} \tag{8}$$

where $\boldsymbol{\tau}_\mathrm{s}$ is the WSS, μ is the variable blood viscosity and $\frac{\partial \mathbf{u}}{\partial \hat{\mathbf{n}}_\mathrm{s}}$ is the velocity gradient in the direction of surface normal.

Oscillatory nature of the blood flow was evaluated by calculating the OSI, as suggested by Ku *et al.*[33]:

$$\mathrm{OSI} = \frac{1}{2}\left(1 - \frac{\left|\frac{1}{T}\int_0^T \bar{\boldsymbol{\tau}}_\mathrm{s} dt\right|}{\frac{1}{T}\int_0^T |\bar{\boldsymbol{\tau}}_\mathrm{s}| dt}\right) \tag{9}$$

where $\bar{\boldsymbol{\tau}}_\mathrm{s}$ is the instantaneous WSS vector ($|\bar{\boldsymbol{\tau}}_\mathrm{s}| = \tau_\mathrm{s}$) and T is the length of the cardiac cycle. OSI is a dimensionless measure that quantifies the departure of the WSS vector from its predominant axial alignment. For purely oscillatory flow, OSI attains the maximum value of 0.5. It is important to note that OSI does not take into account the magnitude of WSS and only considers direction.

The dimensionless endothelial platelet residence time T_r was calculated following conventional approach of Gay and Zhang[21] as:

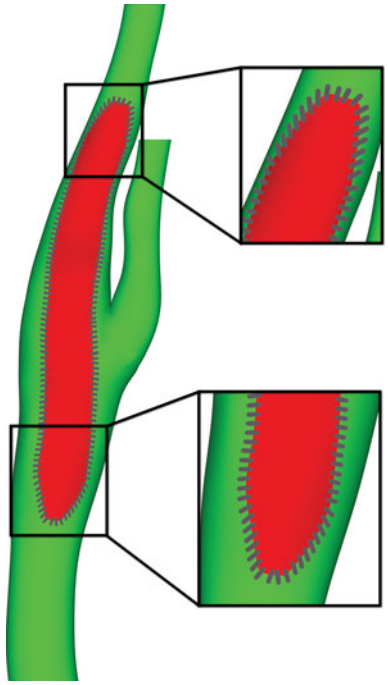

FIGURE 3. Surgical suture incorporated into the model of CEA with anterior patch angioplasty.

$$T_r = \frac{\mu}{T}[(1 - 2\mathrm{OSI})\langle\tau_s\rangle]^{-1} \quad (10)$$

where $\langle\cdot\rangle$ represents the time averaged quantity. It is important to note that T_r is evaluated in the vicinity of the endothelial surface, therefore it does not consider the convection of platelets from/to the core of the flow.

To address this issue, the concept of flow-field coherent vortical structures (VSs) was implemented in conjunction with λ_2 vortex-eduction technique[26] to identify flow regions surrounding a local pressure minimum that may trap the platelets inside.[8] Jeong and Hussain[26] define the VS as a connected region where $\mathbf{D}^2 + \mathbf{\Omega}^2$ has two negative eigenvalues (where $\mathbf{D} = \frac{1}{2}(\Delta\mathbf{u} + (\Delta\mathbf{u})^T)$ and $\mathbf{\Omega} = \frac{1}{2}(\Delta\mathbf{u} - (\Delta\mathbf{u})^T)$ are the rate-of-deformation and rate-of-rotation tensors, respectively). Arranging the eigenvalues as $\lambda_1 > \lambda_2 > \lambda_3$, defines the condition $\lambda_2 < 0$ for the point to belong to the VS. The lasting time of the VS during the cardiac cycle then provides the information on the platelet residence time inside the VS core.

In order to evaluate the cumulative influence of all strain and stress components acting inside the arterial wall, we calculated the CS and ES (or Von Mises stress). CS was computed as the difference between Von Mises strains[50] calculated at peak systole and late diastole:

$$\in_{\mathrm{VM,cyclic}} = \in_{\mathrm{VM,peak\ systole}} - \in_{\mathrm{VM,late\ diastole}} \quad (11)$$

where the Von Mises strain is a strain invariant defined by:

$$\in_{\mathrm{VM}} = \left[\frac{(\in_{\mathrm{I}} - \in_{\mathrm{II}})^2 + (\in_{\mathrm{II}} - \in_{\mathrm{III}})^2 + (\in_{\mathrm{I}} - \in_{\mathrm{III}})^2}{2}\right]^{1/2} \quad (12)$$

and $\in_{\mathrm{I}}, \in_{\mathrm{II}}$ and $\in_{\mathrm{III}}$ are the principal Green strains. ES was calculated using formula (12) substituting strains for stresses. It follows from (11) and (12) that CS quantifies the amount of arterial wall deformation during the cardiac cycle, while ES represents the gross stress response of the artery which is largest during peak systole.

Comparison of Different Types of Patch Angioplasty

OSI and T_r are based on WSS, which means that there are essentially only three independent disease-related factors: WSS, CS and ES, each with its own unique distribution. Separate analysis of these distributions does not provide univocal conclusion on the benefit in all three factors. We therefore introduced the integral Abnormality factor (A_F), which included WSS, CS and ES weighted according to the influence that each factor has on the arterial disease. Though this influence is purely hypothetical and is yet to be clinically validated, we assigned weights to the factors according to the domain they belong to. Namely, WSS (related to hemodynamic mechanism of pathogenesis[11,20]) was assigned a weight of 0.5, while CS and ES (related to injury mechanism of pathogenesis[15,46]) were weighted as 0.25 each:

$$A_F = \frac{A_{\mathrm{WSS}}}{2A_{\mathrm{WSS}}^{\mathrm{eCEA}}} \cdot 100\% + \frac{A_{\mathrm{CS}}}{4A_{\mathrm{CS}}^{\mathrm{eCEA}}} \cdot 100\% + \frac{A_{\mathrm{ES}}}{4A_{\mathrm{ES}}^{\mathrm{eCEA}}} \cdot 100\% \quad (13)$$

where A_{WSS} is the surface area of low temporal mean WSS on the arterial geometry, A_{CS} and A_{ES} are surface areas of high CS (calculated using formulas (11) and (12)) and ES (calculated for peak systole). To put the current findings in the context of our study that compared patch angioplasty to eversion endarterectomy (we found that eversion was superior to CEA with anterior PTFE patch angioplasty in terms of A_F), A_{WSS}, A_{CS} and A_{ES} were normalized to those measured for eversion endarterectomy (eCEA). Thresholds for A_{WSS}, A_{CS} and A_{ES} were selected as follows: WSS: <0.4 Pa,[35] CS: >0.138, ES: >220 kPa (corresponds to >5.34 in the $\log_{10}$ ES contours Fig. 9). Threshold values of CS and ES were chosen based on average CS and ES values observed in all models.

RESULTS

Mathematical models were created for carotid arteries repaired with synthetic PTFE and Dacron, xenogeneic BP, and autologous external jugular and greater saphenous veins. Two types of patch angioplasty (anterior and lateral), and three patch widths were considered [4 mm (narrow), 8 mm (standard) and 16 mm (wide)].

Temporal mean WSS contours (in Pa) are plotted in Fig. 4. Arterial wall was removed from the figure for better visualization of the flow. In all types of patch angioplasty, the area of low WSS (below 0.4 Pa, which is thought to be associated with atherogenic phenotype[35]) was consistently larger on the anterior aspect of the artery than on its posterior side. This phenomenon is particularly salient in the artery with the lateral patch, and is a result of tortuous geometry characterized by the bend in the anterior–posterior plane centered on the carotid bulb. This bend was considerably straightened by the anterior patch angioplasty, which reinforced the anterior aspect of the artery and caused the more compliant wall opposite to the patch to bulge out and increase the area of low WSS posteriorly. The amount of straightening however was not sufficient to

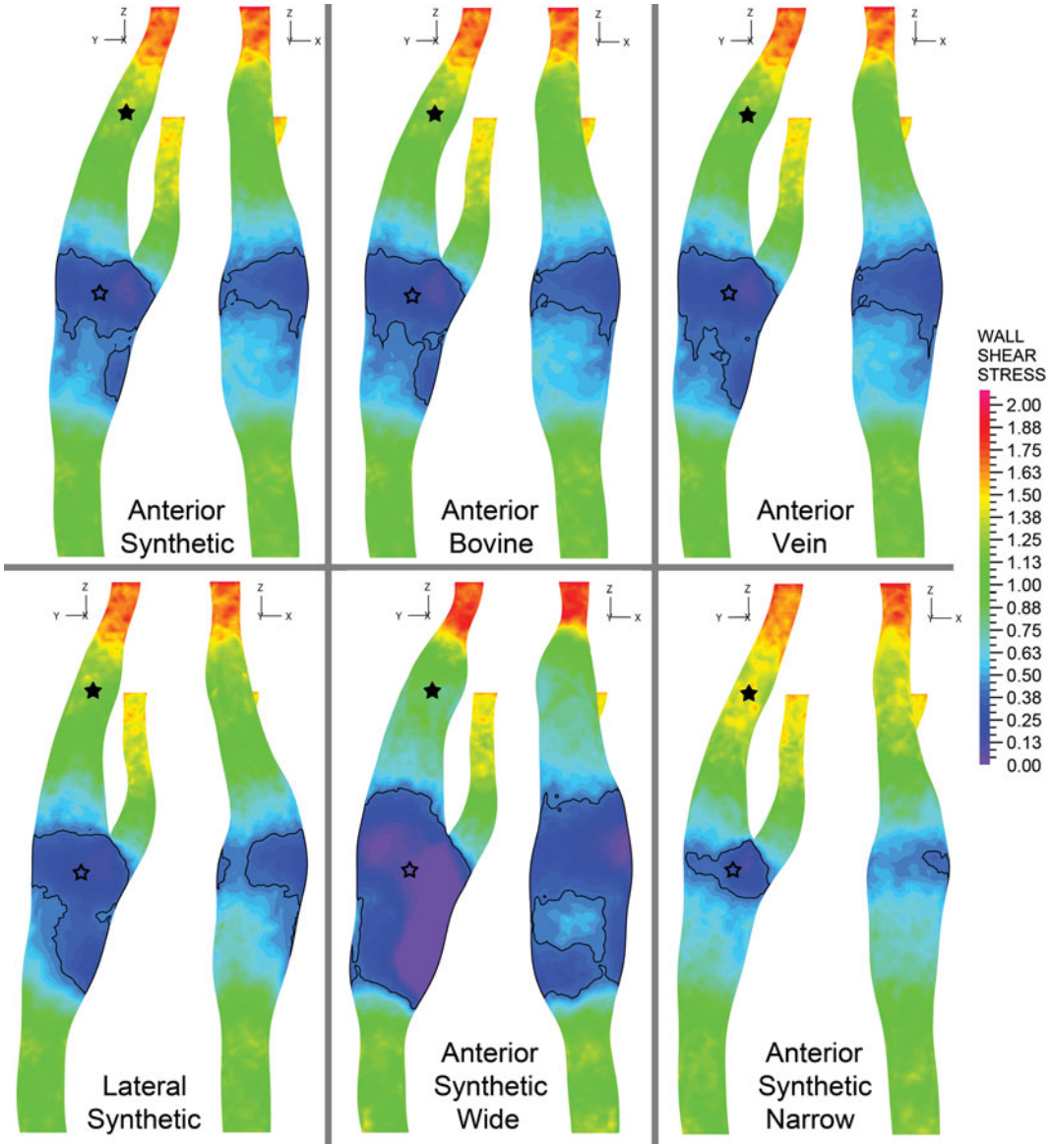

FIGURE 4. Temporal mean WSS (in Pa) contours for anterior and lateral views of the carotid artery repaired with different patch angioplasties. Logarithmic scale is in use. Low WSS (<0.4 Pa[35]) is outlined and represented by shades of dark blue. Stars indicate the locations of WSS measurements used to produce graphs on Fig. 5. Wall of the artery is removed for better visualization.

shift the lowest WSS values from the anterior to the posterior side. This can clearly be seen in the artery with a wide anterior patch. Lateral closure reinforced the artery laterally. This sustained the anterior–posterior bend, but resulted in bulging in the medial direction, creating zone of low WSS proximally.

All types of angioplasty had large continuous region of low WSS in the carotid bulb, while the distal ICA possessed high WSS. Temporal variations of WSS plotted for the center of the carotid bulb and distal ICA (see Fig. 5 for temporal variations and Fig. 4 for locations of measurements) showed that WSS in the bulb did not exceed 0.4 Pa during the entire cardiac cycle. This result was consistent for all patch angioplasties. WSS lower than 0.4 Pa is believed to stimulate the atherogenic phenotype, while values higher than 1.5 Pa induce endothelial quiescence and an atheroprotective gene expression profile.[35]

The OSI contours are plotted in Fig. 6 (left panel). These contours show that flow was oscillatory in the carotid bulb and in the apex. OSI was smaller for CA with lateral patch closure than with anterior patch angioplasty. Variations in patch width resulted in increase in OSI, which was particularly evident for the artery with the wide patch.

Another distinct feature of blood flow in the bulb was reduced blood velocity which increased the endothelial platelet residence time (T_r). Generally, when

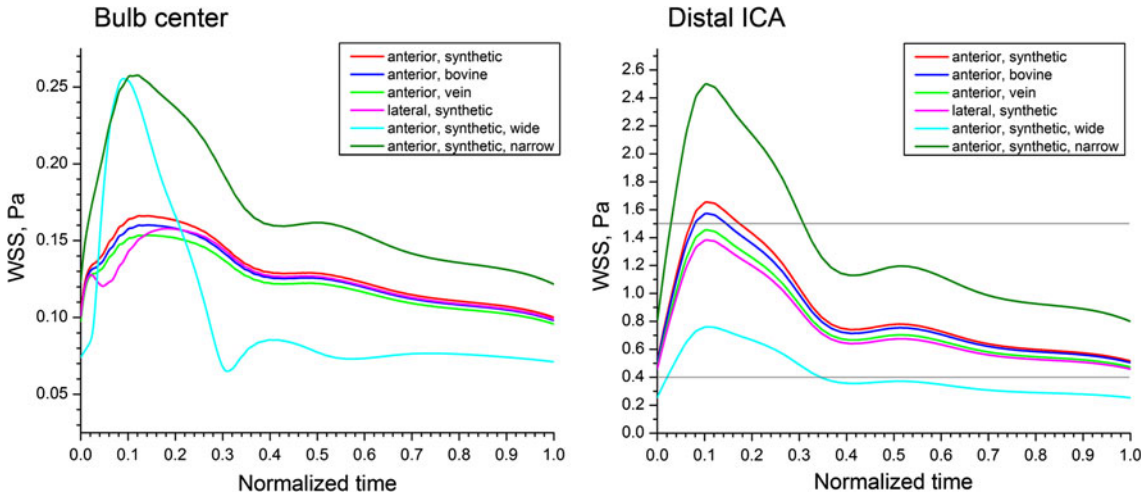

FIGURE 5. Temporal variations of WSS (in Pa) in the center of the carotid bulb (left, location is marked with the hollow star on Fig. 4) and in the distal ICA 3 cm off the carotid apex (right, location is marked with the solid black star on Fig. 4). Values of WSS lower than 0.4 Pa are thought to stimulate the atherogenic phenotype while values higher than 1.5 Pa are reported to induce endothelial quiescence.[35]

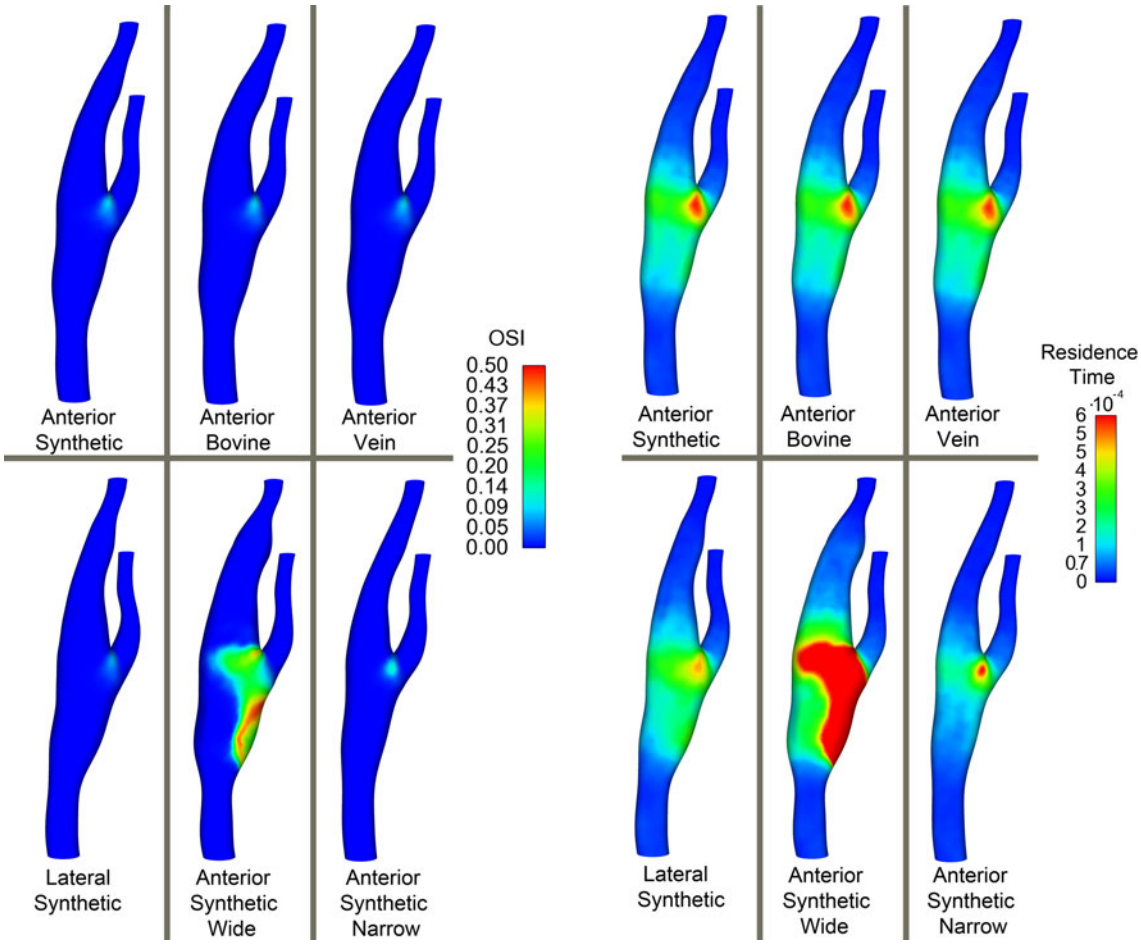

FIGURE 6. Contours of OSI (left) and endothelial platelet residence time T_r (right) for carotid artery repaired with different types of patch angioplasty. The wall of the artery is removed for better visualization of the flow.

OSI is small, it has little effect on T_r.[33] However, as OSI approaches 0.5, T_r dramatically increases. Contours of T_r are plotted in Fig. 6 (right panel). In the vicinity of endothelium, zones where platelets spent more time during the cardiac cycle strongly correlate with areas of low WSS and OSI discussed earlier. Shorter T_r was observed in the model with lateral patch angioplasty than in the model with anterior patch closure, though T_r in the proximal bulb was slightly higher for the former. Decrease of patch width resulted in somewhat shorter endothelial platelet residence times in the apex, while increase in patch width significantly increased T_r in the proximal bulb, especially on its medial aspect.

The core of the flow possessed multiple VS developed predominantly at sites of relatively high WSS and shear rate as seen in Fig. 7. Formation of these vortices was particularly salient during systole, and was associated with variations in lumen size along the arterial axis, resulting in a roll-up of unstable sheets of spanwise vorticity by Kelvin–Helmholtz instability.[8] Larger VSs were seen in arteries with larger bulbs, with the biggest Y-shaped VS observed in the carotid with the wide patch. This Y-shaped VS formed on the medial aspect of the bulb and was present during the first third of the cardiac cycle, after which it was suppressed by the lower flow velocity and shear rate of the diastolic phase. VSs in the proximal CCA and distal ICA and ECA regions with relatively high velocity and shear rate were present during the entire cardiac cycle. In general, Figs. 4, 5, 6, and 7 show that patch material had less effect on WSS, OSI, T_r and VS than the location and especially the size of the patch.

Contours of CS are plotted in Fig. 8. A common feature among all types of angioplasty was high CS in the carotid apex, scattered throughout the bulb, and around the patch at the ends of suture entry in the arterial wall. Latter was due to mismatch in stiffness between the patch and the host wall. This was particularly salient in arteries with stiff synthetic patches (CS of synthetic patches was close to zero), which resulted in bulging of the more compliant wall around the patch. The stiff synthetic patches placed anteriorly straightened the artery in the anterior–posterior direction, which acted favorably for reducing CS on the lateral side. In contrast, lateral patch angioplasty straightened the artery in the lateral-medial direction, which resulted in high CS on the lateral side. In addition, the bend in the anterior–posterior plane centered on the carotid bulb, caused high CS in the distal ICA anteriorly, and in the proximal ICA posteriorly. This can clearly be seen in the artery with lateral patch angioplasty. In CEA with anterior repair, high CS was also present in the ECA close to the carotid apex, with this being on the anterior aspect of the ECA. Use of a more compliant vein or bovine patch acted favorably in reducing CS in this area. Lateral patch angioplasty resulted in relocation of this high CS area from anterior aspect of ECA to its posterior side.

Contours of ES at peak systole are plotted in Fig. 9. Peak systolic values were used as these were the highest during the cardiac cycle and therefore had higher chances for damaging the wall. We plot $\log_{10}$ ES to emphasize the regions of high ES. Colorband values represent orders of 10, i.e., 3 is 1 kPa, 6 is 1 MPa and etc. Similar to CS, high ES in all cases was observed in the carotid apex, scattered throughout the bulb, and at the ends of the suture entry in the wall. In addition, high ES was present on the patch surface. The previously mentioned bulging of the wall opposite to the stiff patch resulted in high ES being circumferentially distributed in the entire area of the bulb. Another feature common to all models was the significantly lower ES on the lateral aspect of the artery (even in the case of lateral patch angioplasty) than on its anterior or posterior sides. Increase of patch width resulted in significant increase in ES on both anterior and posterior aspects of the artery, while decrease in width showed less ES and therefore potential improvement in hemodynamics. Higher compliance of biological patches in comparison to synthetic PTFE and Dacron resulted in less ES and smoother transition of stresses between the arterial wall and the patch.

Abnormality factor (A_F) for all considered models is plotted in Fig. 10. Large A_F represents large areas with abnormal (relative to defined threshold) hemodynamics, smaller A_F represents hemodynamically better results. Figure 10 shows that biological materials (BP and autologous vein) produce better hemodynamics in the repaired artery than synthetic PTFE and Dacron. The main advantage of using the biological patch is in reducing ES (by 20%) and CS (by 1.5–3-fold), which results in overall 12% better A_F.

Lateral angioplasty was superior to anterior angioplasty in terms of ES (lower by 28% for lateral closure), but failed to provide benefits in A_F primarily due to significantly higher CS (higher by 5.8-fold for lateral closure). Effect of patch width on the hemodynamics of the repaired artery was significantly more salient than the effect of patch material. Increase of patch width by a factor of two, resulted in 2.2-fold higher A_F, while decrease of the path width by a factor of two, resulted in 68% smaller A_F.

DISCUSSION

Multiple randomized controlled clinical trials have been conducted comparing the effects of patch closure

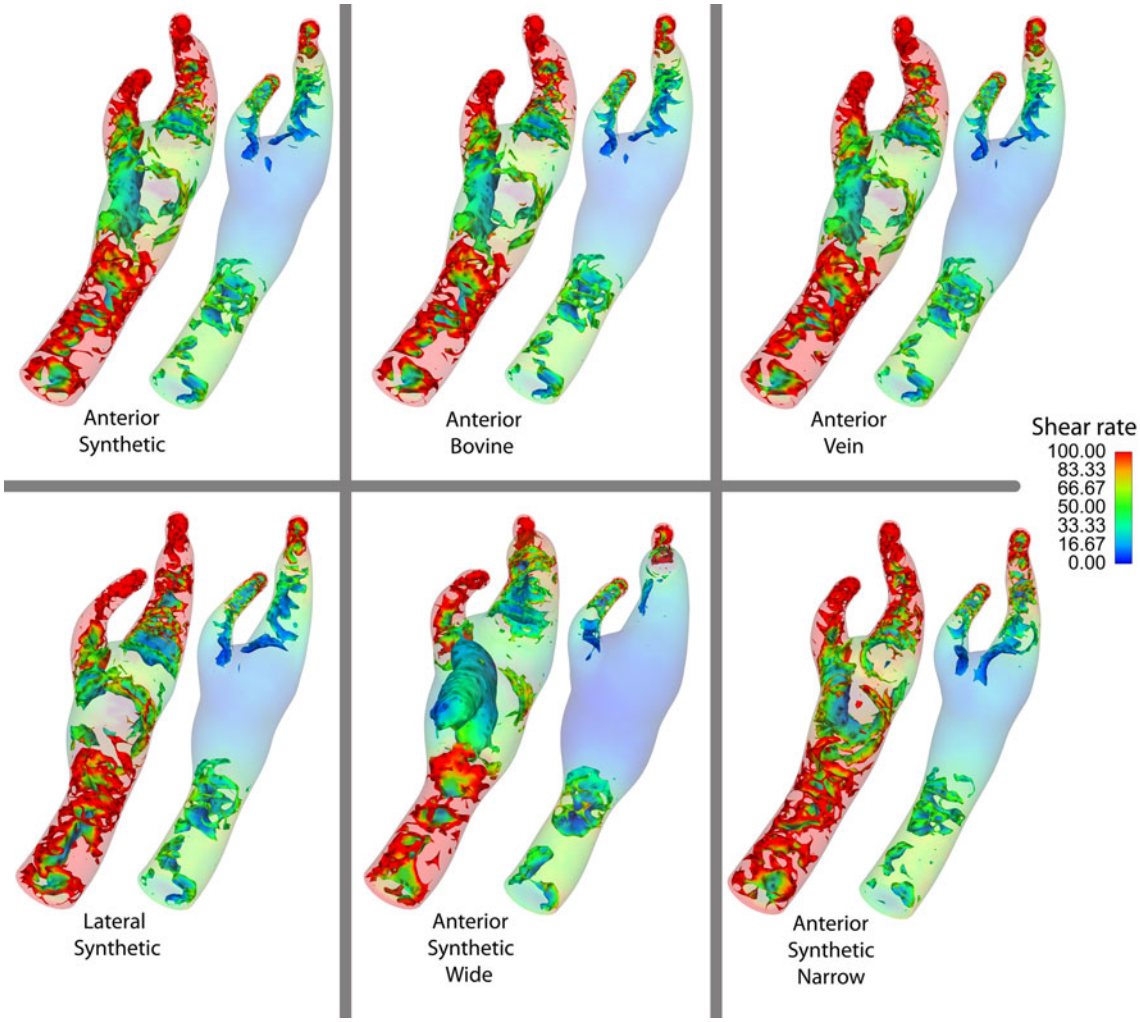

FIGURE 7. VS at peak systole (left) and late diastole (right) for carotid artery repaired with different types of patch angioplasty. VSs are colored with scalar shear rate (s^{-1}) and were educed with λ_2-method of Jeong and Hussain[26] using threshold value of $\lambda_2 = -20\ s^{-2}$. Wall of the artery is removed for better visualization.

on perioperative stroke and death rates, and long-term restenosis.[1,2,9,10,22,36,39,41,42,48] Clinical results have varied among the trials, and controversy still remains regarding the best material for patch angioplasty after CEA.[9,10,39] With the help of mathematical modeling, we analyzed and compared the effects of different materials, and studied the influence of patch width and location of arteriotomy on the hemodynamics of the repaired carotid artery.

Performed analysis showed that none of the existing patch materials seem to provide atheroprotective hemodynamics. The atheroprotective hemodynamics is believed to be impacted by physiological and elevated shear (values higher than 1–2 Pa,[35] but lower than 40 Pa[24]). High shear renders endothelium less susceptible to pathogenic stimuli of injury, cell adhesion, cell proliferation, and lipid uptake.[35] Proximal CCA and distal ICA and ECA generally have high shear and rare clinical findings of carotid disease. At the same time, high shear may lead to platelet activation by von Willebrand factor,[47] especially in the absence of antagonists from the altered endothelial layer. The high-shear-stress activated platelets may then get trapped in the low-shear-stress areas.[8] Low shear (below 0.4 Pa) is thought to switch the endothelial phenotype from atheroprotective to atherogenic[35] and is believed to be involved with mediated recruitment of monocytes; increased vasoconstriction and paracrine growth stimulation of vessel wall constituents; increased oxidant state; and increased apoptosis and cellular turnover.[35] Zones of low wall shear were present in all considered types of patch angioplasty, with the largest zone observed in the artery with a wide synthetic patch placed anteriorly. This was attributed to a significantly wider bulb, and also a more acute transition from the patch to the native artery. The

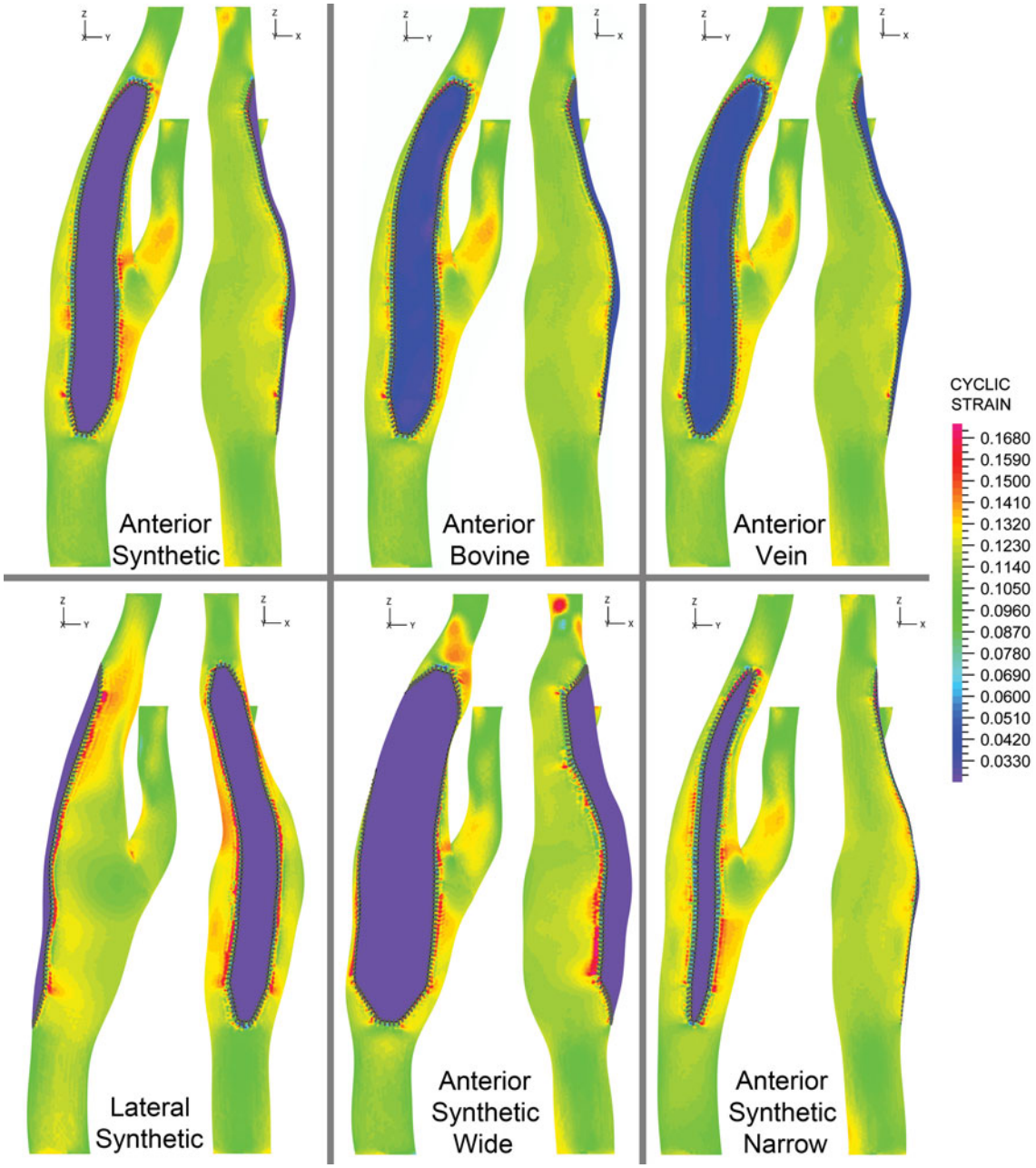

FIGURE 8. CS for anterior and lateral views of carotid artery repaired with different types of patch angioplasty.

carotid bulb is known to be one of the first sites in the carotid bifurcation to develop atherosclerotic inflammation.[33] Due to an abrupt change in the curvature and a sudden increase in cross-sectional area at the carotid bulb, high momentum blood is incapable of instantaneously changing direction to accommodate the curvature. This is most pronounced during systole, when the flow exhibits boundary layer separation and formation of VSs. High WSS and the trapping effect of salient VSs during systole may activate the platelets[8] and promote their deposition in the arterial wall when they get into the slow viscous diastolic flow of the bulb. Clinical studies have supported this conclusion by demonstrating clinical complications in arteries repaired with wide patches. These complications include distal ICA kinks, excessive posterior wall mural thrombus formation[27] and overall higher rates of recurrent stenosis.[4]

Artery with a narrow patch angioplasty on the other hand showed significant improvement in hemodynamics. It is however important to note that the key aspect of this improvement is most likely the smooth transition from the angioplasty site to the non-endarterectomized wall. Mean carotid artery geometry

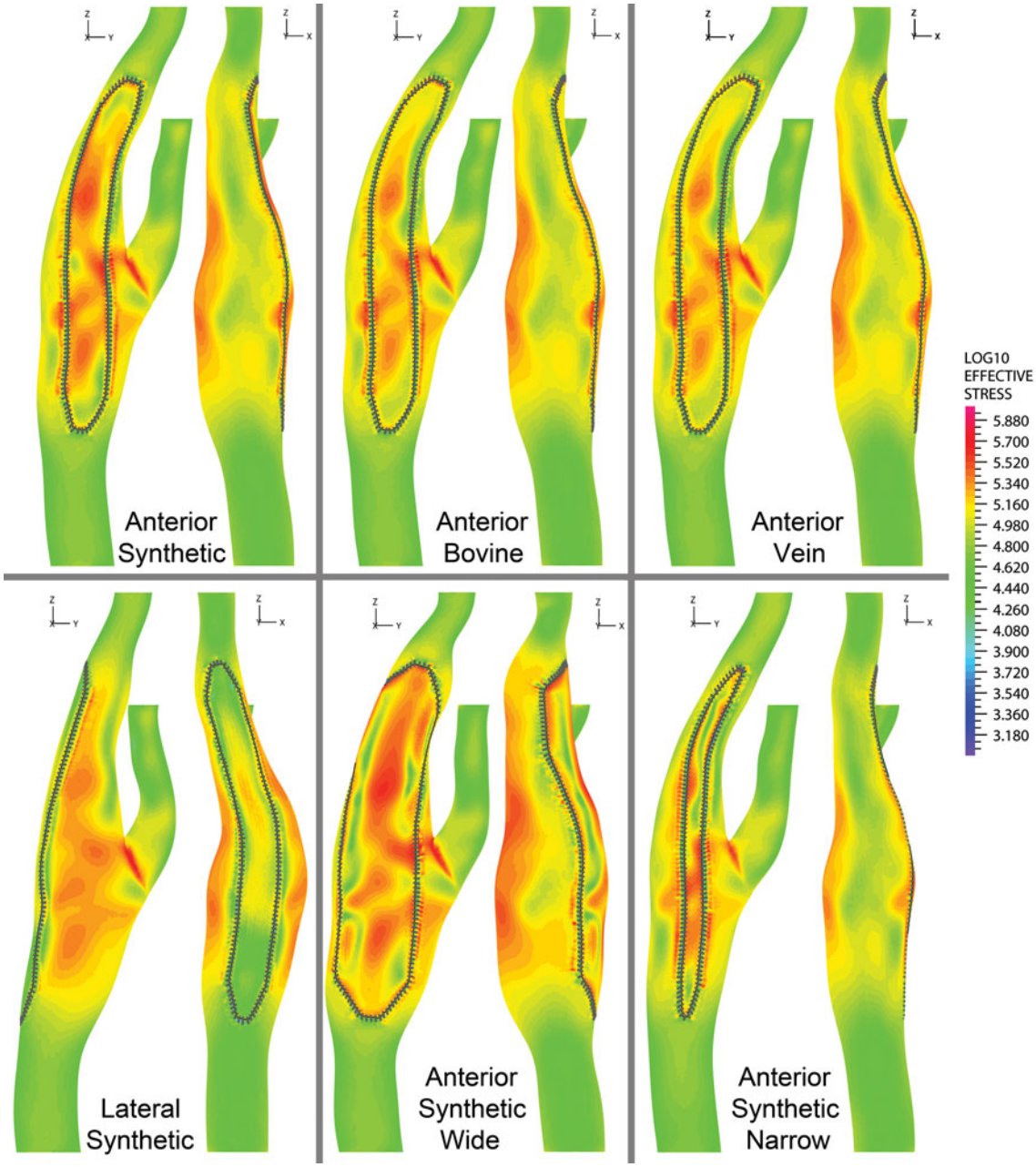

FIGURE 9. ES at peak systole for anterior and lateral views of carotid artery repaired with different types of patch angioplasty. Common logarithm of ES is plotted to emphasize the differences between high and low values.

considered in this study had the bulb that was sufficiently large to prevent taper in the distal ICA after angioplasty. It is possible, however, that in a particular patient-specific case with a smaller bulb, use of a narrow patch may result in such a taper. This may then entail the same hemodynamic problems as the wide patch angioplasty.

Location of arteriotomy was found to have significant effect on the arterial hemodynamics. Lateral patch closure showed improvement in ES compared to the anterior angioplasty. However, this improvement was overtrumped by significantly higher CS in the CEA with lateral patch closure.

Results of modeling have shown that patch material had less pronounced effect on hemodynamics than the size of the patch or location of arteriotomy. All patch materials caused stress concentrations in the bulb of the repaired artery, which is consistent with the clinical findings of Rosenthal *et al.*[45] demonstrating higher incidence of post CEA restenosis at this location. Better results were achieved for arteries repaired with biological materials (BP and autologous veins) than

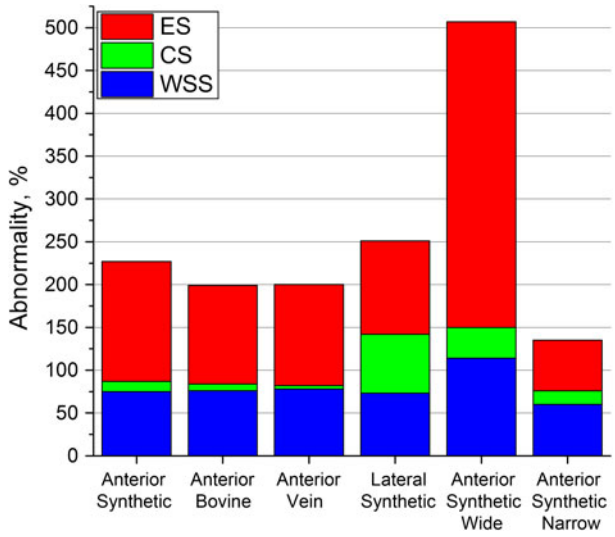

FIGURE 10. Abnormality factor (%) calculated for carotid artery repaired with different types of patch angioplasty. Smaller values represent hemodynamically better results.

for their synthetic substitutes (PTFE and Dacron). This was primary due to smaller mismatch in stiffness between the biological patch and the host arterial wall, which resulted in lower values of ES and its smoother transition from the patch to the wall. Smaller stress suggests lower risk of wall injury and therefore lower incidence of recurrent stenosis.

Patching with autologous venous tissue remains the most commonly used option for closing the arteriotomy after carotid endarterectomy.[39] The veins most commonly used are the greater saphenous and external jugular.[7] Saphenous vein is harvested from the patient's thigh or ankle which requires a separate incision and therefore causes additional trauma to the patient. External jugular vein does not require a separate incision but is substantially thinner than saphenous vein which raises concerns of this patch becoming aneurismal with subsequent complications related to thrombosis or rupture. To avoid rupture or aneurismal expansion, some surgeons use the external jugular vein in a double-walled configuration.

Results of our study suggest that wide patches have significant ES concentrations on their surface, and therefore may more likely rupture than a narrow patch. Though unlikely for synthetic patches (due to their high strength), this may be important to keep in mind when using a wide vein patch. Such ruptures, when occurring, have been associated with high rates of patient death or severe disability.[55] An alternative to a vein patch may be the BP. In this study bovine patches have shown similar hemodynamic results to vein patches. They were also reported to be superior to their synthetic counterparts in terms of restenosis, stroke and death rates by several clinical studies.[22,36]

CONCLUSION

There is a considerable debate over the type, size and location of the patch to be used for the performance of carotid endarterectomy. This work presents an effort to compare commonly used synthetic and biological materials, and to evaluate the influence of patch size and location of arteriotomy on the hemodynamics of the repaired artery. The mathematical models presented in this study account for the three-dimensional mean arterial geometry, fluid–structure interaction, non-linear anisotropic properties of the arterial wall, non-Newtonian blood rheology, and *in vivo* boundary conditions.

Analysis of hemodynamics showed that patch angioplasties performed with autologous vein and BP were superior to CEA with synthetic patch closure in terms of restenosis potential. Width of the patch and location of arteriotomy were found to be of paramount importance, with narrow patches being superior to wide patches, and anterior arteriotomy being superior to lateral arteriotomy. Though thorough clinical validation of these findings is required, the results of the present analysis are envisaged to aid not only in the understanding of pathophysiology of the repaired carotid bifurcation, but also in choice of the type of patch angioplasty.

ACKNOWLEDGMENTS

This work was supported in part by NIH grants K08HL079967 and R01AG034995 and by the grants from Nebraska Research Initiative Nanofiber Core Facility, National Science Foundation, and UNL/UNMC Engineering for Medicine initiative.

REFERENCES

[1]AbuRahma, A. F., P. A. Robinson, S. Saiedy, J. H. Kahn, and J. P. Boland. Prospective randomized trial of carotid endarterectomy with primary closure and patch angioplasty with saphenous vein, jugular vein, and polytetrafluoroethylene: long-term follow-up. *J. Vasc. Surg.* 27(2):222–234, 1998.

[2]AbuRahma, A. F., P. A. Stone, S. K. Flaherty, and Z. AbuRahma. Prospective randomized trial of Acuseal (Gore-Tex) versus Hemashield-Finesse patching during carotid endarterectomy: early results. *J. Vasc. Surg.* 45(5):881–884, 2007.

[3]American College of Cardiology Foundation, American Society of Interventional & Therapeutic Neuroradiology, Society for Cardiovascular Angiography, Interventions, Society for Vascular Medicine, Biology, Society of Interventional Radiology, E. R. Bates, J. D. Babb, D. E. Casey, C. U. Cates, G. R. Duckwiler, T. E. Feldman, W. A. Gray,

K. Ouriel, E. D. Peterson, K. Rosenfield, J. H. Rundback, R. D. Safian, M. A. Sloan, and C. J. White. ACCF/SCAI/SVMB/SIR/ASITN 2007 clinical expert consensus document on carotid stenting: a report of the American College of Cardiology Foundation task force on clinical expert consensus documents (ACCF/SCAI/SVMB/SIR/ASITN clinical expert consensus document committee on carotid stenting). *J. Am. Coll. Cardiol.* 49(1):126–170, 2007.

[4]Archie, J. P. How can I achieve the optimal flow surface and distal end-point following carotid endarterectomy? In: Carotid Artery Surgery: A Problem-Based Approach, edited by R. A. Naylor and W. C. Mackey. London: Harcourt, 1999, pp. 262–270.

[5]Awad, I. A., and J. R. Little. Patch angioplasty in carotid endarterectomy. Advantages, concerns, and controversies. *Stroke*. 20(3):417–422, 1989.

[6]Bathe, K. J. Finite Element Procedures. Englewood Cliffs, NJ: Prentice Hall, 1996.

[7]Berguer, R., and E. Kieffer. Surgery of the Arteries to the Head. Heidelberg: Springer, 1992.

[8]Biasetti, J., F. Hussain, and T. C. Gasser. Blood flow and coherent vortices in the normal and aneurysmatic aortas: a fluid dynamical approach to intraluminal thrombus formation. *J. R. Soc. Interface* 8:1449–1461, 2011.

[9]Bond, R., K. Rerkasem, A. R. Naylor, A. F. Aburahma, and P. M. Rothwell. Systematic review of randomized controlled trials of patch angioplasty versus primary closure and different types of patch materials during carotid endarterectomy. *J. Vasc. Surg.* 40(6):1126–1135, 2004.

[10]Bond, R., K. Rerkasem, R. Naylor, and P. M. Rothwell. Patches of different types for carotid patch angioplasty. *Cochrane Database Syst. Rev.* 2:CD000071, 2004.

[11]Caro, C. G., J. M. Fitz-Gerald, and R. C. Schroter. Atheroma and arterial wall shear. observation, correlation and proposal of a shear dependent mass transfer mechanism for atherogenesis. *Proc. R. Soc. Lond. B Biol. Sci.* 177(46):109–159, 1971.

[12]Chatzizisis, Y. S., A. U. Coskun, M. Jonas, E. R. Edelman, C. L. Feldman, and P. H. Stone. Role of endothelial shear stress in the natural history of coronary atherosclerosis and vascular remodeling: molecular, cellular, and vascular behavior. *J. Am. Coll. Cardiol.* 49(25):2379–2393, 2007.

[13]Chien, S. Biophysical behavior of red cells in suspensions. *Red Blood Cell* 2:1031–1133, 1975.

[14]Cho, Y. I., and K. R. Kensey. Effects of the non-Newtonian viscosity of blood on flows in a diseased arterial vessel. Part 1: steady Flows. *Biorheology* 28:241–262, 1991.

[15]Clowes, A. W., M. A. Reidy, and M. M. Clowes. Mechanisms of stenosis after arterial injury. *Lab. Invest.* 49(2):208–215, 1983.

[16]Conklin, B. S., R. P. Vito, and C. Chen. Effect of low shear stress on permeability and occludin expression in porcine artery endothelial cells. *World J. Surg.* 31(4):733–743, 2007.

[17]De Letter, J. A., F. L. Moll, R. J. Welten, B. C. Eikelboom, R. G. Ackerstaff, F. E. Vermeulen, and A. Algra. Benefits of carotid patching: a prospective randomized study with long-term follow-up. *Ann. Vasc. Surg.* 8(1):54–58, 1994.

[18]Fischer, P. F., F. Loth, S. E. Lee, S.-W. Lee, D. S. Smith, and H. S. Bassiouny. Simulation of high-reynolds number vascular flows. *Comput. Methods Appl. Mech. Eng.* 196:3049–3060, 2007.

[19]Fox, A. J. How to measure carotid stenosis. *Radiology* 186(2):316–318, 1993.

[20]Fry, D. L. Mathematical models of arterial transmural transport. *Am. J. Physiol.* 248(2 Pt 2):H240–H263, 1985.

[21]Gay, M., and L. T. Zhang. Numerical studies of blood flow in healthy, stenosed, and stented carotid arteries. *Int. J. Numer. Methods Fluids* 61(4):453–472, 2009.

[22]Hines, G. L., M. Feuerman, D. Cappello, and V. Cruz. Results of carotid endarterectomy with pericardial patch angioplasty: rate and predictors of restenosis. *Ann. Vasc. Surg.* 21(6):767–771, 2007.

[23]Holzapfel, G. A., T. C. Gasser, and R. W. Ogden. A new constitutive framework for arterial wall mechanics and a comparative study of material models. *J. Elasticity* 61:1–48, 2000.

[24]Humphrey, J. D. Cardiovascular Solid Mechanics: Cells, Tissues, and Organs. New York: Springer, 2002.

[25]Hunter, K. S., C. J. Lanning, S.-Y. J. Chen, Y. Zhang, R. Garg, D. D. Ivy, and R. Shandas. Simulations of congenital septal defect closure and reactivity testing in patient-specific models of the pediatric pulmonary vasculature: a 3D numerical study with fluid-structure interaction. *J. Biomech. Eng.* 128(4):564–572, 2006.

[26]Jeong, J., and F. Hussain. On the identification of a vortex. *J. Fluid Mech.* 285:69–94, 1995.

[27]Johnson, B. L., A. K. Gupta, D. F. Bandyk, C. Shulman, and M. Jackson. Anatomic patterns of carotid endarterectomy healing. *Am. J. Surg.* 172(2):188–190, 1996.

[28]Johnston, B. M., P. R. Johnston, S. Corney, and D. Kilpatrick. Non-Newtonian blood flow in human right coronary arteries: steady state simulations. *J. Biomech.* 37(5):709–720, 2004.

[29]Kamenskiy, A. V., Y. A. Dzenis, J. N. MacTaggart, A. S. Desyatova, and I. I. Pipinos. In vivo three-dimensional blood velocity profile shapes in the human common, internal and external carotid arteries. *J. Vasc. Surg.* 54:1011–1020, 2011.

[30]Kamenskiy, A. V., Y. A. Dzenis, J. N. MacTaggart, and I. I. Pipinos. Three-dimensional geometry of the human carotid artery. *J. Biomech. Eng.* 134(6):064502, 2012.

[31]Kamenskiy, A. V., I. I. Pipinos, A. S. Desyatova, Y. E. Salkovskiy, L. Y. Kossovich, I. V. Kirillova, L. A. Bockeria, K. M. Morozov, V. O. Polyaev, T. G. Lynch, and Y. A. Dzenis. Finite element model of the patched human carotid. *Vasc. Endovasc. Surg.* 43:533–541, 2009.

[32]Kamenskiy, A. V., I. I. Pipinos, J. N. MacTaggart, S. A. J. Kazmi, and Y. A. Dzenis. Comparative analysis of the biaxial mechanical behavior of carotid wall tissue and biological and synthetic materials used for carotid patch angioplasty. *J. Biomech. Eng.* 133(11):111008, 2011.

[33]Ku, D. N., D. P. Giddens, C. K. Zarins, and S. Glagov. Pulsatile flow and atherosclerosis in the human carotid bifurcation. Positive correlation between plaque location and low oscillating shear stress. *Arteriosclerosis.* 5(3):293–302, 1985.

[34]Lee, S. E., S.-W. Lee, P. F. Fischer, H. S. Bassiouny, and F. Loth. Direct numerical simulation of transitional flow in a stenosed carotid bifurcation. *J. Biomech.* 41(11):2551–2561, 2008.

[35]Malek, A. M., S. L. Alper, and S. Izumo. Hemodynamics shear stress and its role in atherosclerosis. *JAMA.* 282(21):2035–2042, 1999.

[36]Marien, B. J., J. D. Raffetto, C. S. Seidman, W. W. LaMorte, and J. O. Menzoian. Bovine pericardium vs Dacron for patch angioplasty after carotid endarterectomy: a prospective randomized study. *Arch. Surg.* 137(7):785–788, 2002.

[37]Maurits, N. M., G. E. Loots, and A. E. P. Veldman. The influence of vessel wall elasticity and peripheral resistance

on the carotid artery flow wave form: a CFD model compared to in vivo ultrasound measurements. *J. Biomech.* 40:427–436, 2007.
[38]Moore, W. S. Extracranial cerebrovascular disease: the carotid artery. In: Vascular Surgery: A Comprehensive Review, edited by W. S. Moore. Philadelphia: WB Saunders, 1983, pp. 617–658.
[39]Muto, A., T. Nishibe, H. Dardik, and A. Dardik. Patches for carotid artery endarterectomy: current materials and prospects. *J. Vasc. Surg.* 50(1):206–213, 2009.
[40]Myers, S. I., R. J. Valentine, A. Chervu, B. L. Bowers, and G. P. Clagett. Saphenous vein patch versus primary closure for carotid endarterectomy: long-term assessment of a randomized prospective study. *J. Vasc. Surg.* 19(1):15–22, 1994.
[41]Naylor, R., P. D. Hayes, D. A. Payne, H. Allroggen, S. Steel, M. M. Thompson, N. J. M. London, and P. R. F. Bell. Randomized trial of vein versus dacron patching during carotid endarterectomy: long-term results. *J. Vasc. Surg.* 39(5):985–993, 2004.
[42]O'Hara, P. J., N. R. Hertzer, E. J. Mascha, L. P. Krajewski, D. G. Clair, and K. Ouriel. A prospective, randomized study of saphenous vein patching versus synthetic patching during carotid endarterectomy. *J. Vasc. Surg.* 35(2):324–332, 2002.
[43]Ricotta, J. J., and M. Piazza. Carotid endarterectomy or carotid artery stenting? Matching the patient to the intervention. *Perspect. Vasc. Surg. Endovasc. Ther.* 22(2):124–136, 2010.
[44]Rockman, C. B., E. A. Halm, J. J. Wang, M. R. Chassin, S. Tuhrim, P. Formisano, and T. S. Riles. Primary closure of the carotid artery is associated with poorer outcomes during carotid endarterectomy. *J. Vasc. Surg.* 42(5):870–877, 2005.
[45]Rosenthal, D., J. P. Archie, M. H. Avila, D. F. Bandyk, J. D. Carmichael, G. P. Clagett, J. L. Hamman, H. M. Lee, P. R. Liebman, J. L. Mills, S. L. Minken, G. W. Plonk, M. P. Posner, R. B. Smith, and S. T. String. Secondary recurrent carotid stenosis. *J. Vasc. Surg.* 24(3):424–429, 1996.
[46]Ross, R. The pathogenesis of atherosclerosis: a perspective for the 1990 s. *Nature.* 362(6423):801–809, 1993.
[47]Ruggeri, Z. M., and G. L. Mendolicchio. Adhesion Mechanisms In Platelet Function. *Circ. Res.* 100:1673–1685, 2007.
[48]Saad, E. M., H. Sharaf, A. A. El-Latif, K. Mowafy, and A. Al-Mongy. Carotid endarterectomy: primary closure versus patch angioplasty. *Egypt. J. Surg.* 22(1):59–68, 2003.
[49]Selzer, R. H., H. N. Hodis, H. Kwong-Fu, W. J. Mack, P. L. Lee, C. R. Liu, and C. H. Liu. Evaluation of computerized edge tracking for quantifying intima-media thickness of the common carotid artery from b-mode ultrasound images. *Atherosclerosis.* 111(1):1–11, 1994.
[50]Shigley, J. E., and C. R. Mischke. Mechanical Engineering Design. New York: McGraw-Hill, 1989.
[51]Sumpio, B. E. Hemodynamic forces and the biology of the endothelium: signal transduction pathways in endothelial cells subjected to physical forces in vitro. *J. Vasc. Surg.* 13(5):744–746, 1991.
[52]Tambasco, M., and D. A. Steinman. Path-dependent hemodynamics of the stenosed carotid bifurcation. *Ann. Biomed. Eng.* 31:1054–1065, 2003.
[53]Tontonoz, P., L. Nagy, J. G. Alvarez, V. A. Thomazy, and R. M. Evans. Ppargamma promotes monocyte/macrophage differentiation and uptake of oxidized LDL. *Cell.* 93(2):241–252, 1998.
[54]Tropea, B. I., S. P. Schwarzacher, and A. Chang. Reduction of aortic wall motion inhibits hypertension-mediated experimental atherosclerosis. *Artherioscler. Thromb. Vasc. Biol.* 20:2127–2133, 2000.
[55]Yamamoto, Y., D. G. Piepgras, W. R. Marsh, and F. B. Meyer. Complications resulting from saphenous vein patch graft after carotid endarterectomy. *Neurosurgery.* 39(4):670–675, 1996.
[56]Younis, H. F., M. R. Kaazempur-Mofrad, R. C. Chan, A. G. Isasi, D. P. Hinton, A. H. Chau, L. A. Kim, and R. D. Kamm. Hemodynamics and wall mechanics in human carotid bifurcation and its consequences for atherosclerosis: investigation of inter-individual variation. *Biomech. Model. Mechanobiol.* 3:17–32, 2004.